doi.org/10.36721/PJPS.2026.39.5.REG.13646.1

Inhibitory effect of vemurafenib combined with panobinostat on human anaplastic thyroid cancer cells

Yang Li[1#], Han Gao[2#], Peng Zhang[3], Wenjun Wang[3], Jianwen Zhou[1], Jing Cui[1], Di Xue[1], Baofeng Zhang[3], Peihong Li[3], Li Fan[1]* and Jingwei Xu[3]*

[1]Research Institute of Medicine and Pharmacy of Qiqihar Medical University, Qiqihar, China
[2]Medical Technology Academy of Qiqihar Medical University, Qiqihar, China
[3]Department of General Surgery 1, The First Affiliated Hospital of Qiqihar Medical University, Qiqihar, China

Abstract: **Background**: Anaplastic thyroid cancer (ATC) is a highly malignant tumor with poor prognosis and limited therapeutic options, creating an urgent need for novel treatments. **Objectives**: This study aimed to investigate the inhibitory effect of Vemurafenib (Ve) combined with Panobinostat (Pa) on human ATC cells (FRO and ARO) and its underlying mechanism. **Methods**: Four groups were established: Control, Ve, Pa, and Ve+Pa. Cell proliferation and drug synergy were analyzed using CCK-8 assay, colony formation assay, and CompuSyn software. Cell migration, invasion, apoptosis, and glucose consumption were detected by Transwell assay, wound healing assay, apoptosis assay, and glucose consumption assay, respectively. Molecular markers were examined via RT-qPCR, Western blotting, and immunofluorescence. **Results**: CompuSyn analysis verified the synergistic effect of Ve+Pa in FRO and ARO cells. Compared with the other three groups, the Ve+Pa group showed significantly suppressed cell proliferation, migration, invasion, and glucose consumption, as well as enhanced apoptosis. Moreover, the mRNA and protein expression of the sodium iodide symporter (NIS) and iodine metabolism-related molecules was upregulated, whereas glucose transporter 1 (GLUT1) expression was downregulated. **Conclusion**: Ve combined with Pa exerts a synergistic inhibitory effect on the growth and metastasis of FRO and ARO cells, while promoting apoptosis and cellular redifferentiation. This combination may provide a potential therapeutic strategy for ATC.

Keywords: Anaplastic thyroid cancer cells; GLUT1; NIS; Panobinostat; Vemurafenib

Submitted on 05-11-2024 – Revised on 08-08-2025 – Accepted on 01-10-2025

INTRODUCTION

Thyroid cancer (TC) is a common malignant tumor of the head and neck, accounting for 1%-2% of all malignant tumors in the body, with a female predominance (Mihailovic *et al*., 2021). Its main pathological subtypes include papillary, follicular, anaplastic and medullary thyroid carcinomas (Boucai *et al*., 2024). Among these subtypes, ATC is relatively rare but highly aggressive. It is difficult to cure with conventional treatments and has a poor prognosis, with most patients presenting extensive local invasion or distant metastasis (Lawless *et al*., 2024). Therefore, exploring effective treatments for ATC is of particular significance.

Currently, targeted therapy is used in two scenarios: As neoadjuvant therapy for unresectable tumors and for the treatment of metastatic or unresectable disease (Scheffel *et al*., 2022). In ATC, treatments targeting specific molecular pathways-such as epidermal growth factor receptor (EGFR), peroxisome proliferator-activated receptor γ (PPAR-γ), and mammalian target of rapamycin (mTOR) inhibitors-have demonstrated clinical efficacy (Durai *et al*., 2021).

In TC, mutations in the B-Raf proto-oncogene serine/threonine kinase (BRAF) gene are the most common within the mitogen-activated protein kinase (MAPK) signaling pathway, with the predominant alteration being a point mutation at position 600, where valine is substituted by glutamate ($BRAF^{V600E}$) (Lu *et al*., 2022; Su *et al*., 2021). BRAF mutations are associated with reduced expression of genes involved in thyroid iodine metabolism, upregulation of glucose metabolism-related genes, and inhibition of TC cell differentiation (Pliszka *et al*., 2021). Ve is a small-molecule inhibitor targeting $BRAF^{V600E}$ (Kopetz *et al*., 2021). In the treatment of TC, it can upregulate the expression of thyroid cancer-specific genes by inhibiting the MAPK pathway, thereby restoring radioiodine (RAI) uptake in radioiodine-refractory differentiated TC (RAIR-DTC) caused by BRAF mutations (Faria *et al*., 2021). However, single-agent therapy has limited efficacy and acts through a single signaling pathway. Therefore, combining it with other inhibitors can enhance the anti-thyroid cancer effect and overcome the limitations of a single target pathway and limited mechanistic links. Studies have indicated that histone deacetylase (HDAC) inhibitors can significantly induce the expression of the NIS gene in breast cancer (BC) cells (Rathod *et al*., 2024). Pa is a novel HDAC inhibitor (Bhutkar *et al*., 2024). When combined with melphalan, it exerts a synergistic anti-multiple myeloma effect (Chang *et al*., 2023). However, research regarding its application in the treatment of ATC

**Corresponding author:* e-mail: fan123456li@126.com; xjw2020@126.com
#These authors contributed equally and are the co-first authors.

remains scarce. In light of this, the present study combined the BRAF inhibitor vemurafenib with the HDAC inhibitor Pa to treat FRO and ARO cells. The purpose was to examine whether this combination regimen demonstrates greater efficacy than monotherapy in inhibiting tumor cell growth and inducing redifferentiation, and to provide a more favorable therapeutic option for clinical practice.

MATERIALS AND METHODS

Cell culture and medicine

The cells utilized in this experiment were all ATC cells. Specifically, FRO and ARO cell lines were obtained from the Shanghai Institute of Life Sciences. Ve (No. BCPD2326) and Pa (No. BCP01816) were purchased from Hanxiang Biotechnology, China.

Instruments and Equipment

Microplate Reader (Tecan, Model: SPARK), Flow Cytometer (BD, Model: FACSCalibur), Laser Scanning Confocal Microscopy (Zeiss, Model: LSM710), Real-time qPCR System (ABI, Model: Q5), Gel Imaging System (BioRad, Model: WFH-102).

Cell viability analysis

FRO and ARO cells were seeded in 96-well plates, and the medium was aspirated the next day. The cells were treated with various concentrations of Ve (6.25, 12.5, 25, 50, 100 μM for FRO cells; 4, 8, 16, 32, 64 μM for ARO cells) and Pa (2, 4, 8, 16, 32 μM for FRO cells; 1, 2, 4, 8, 16 μM for ARO cells) were used to treat the cells. Control cells received an equivalent volume of DMSO. After 24 h of treatment, 10 μL of CCK-8 solution was added to each well, followed by incubation at 37°C for 2 h. The absorbance at 450 nm was measured using a microplate reader and the IC50 values were calculated accordingly (Hu *et al*., 2023) .

Drug combination analysis

Based on the dose-response curve calculations, Vemurafenib and Panobinostat were combined at a specific ratio for treating FRO and ARO cells. The synergistic effect of the combination was analyzed using CompuSyn software (Ismail *et al*., 2025), which directly calculated the combination index (CI), growth inhibition rate (Fa), and dose reduction index (DRI) based on the input data. To quantify the drug-drug interaction effects, an isobologram was generated.

Plate cloning and wound healing assay

FRO and ARO cells were seeded in six-well plates at a density of 600 cells per well, respectively. Ve (12.5 μM) and Pa (4 μM) were applied alone or in combination to FRO cells; Ve (4 μM) and Pa (1 μM) were applied alone or in combination to ARO cells and the solution was changed every three days until the tenth day. The old solution was discarded, methanol was added for fixation and crystal violet staining, the well plates were photographed and the clone formation rate was calculated. For the wound healing assay, 3.0×10^5 cells were inoculated into six-well plates. After the cells had fully adhered and confluent in the wells overnight, a uniform scratch was made in the cell monolayer using a 200 μL pipette tip. The wells were then washed three times with PBS, supplemented with culture medium, and incubated for 24 h, followed by the determination of the wound healing rate.

Transwell chambers assay

Cells were grouped and treated as described above. For the migration assay, 800 μL of cell suspension was added to the Transwell inserts. For the cell invasion assay, Transwell inserts pre-coated with Matrigel were placed into 24-well plates, with culture medium added to both the upper and lower chambers.After 24 h of incubation, the inserts were removed and the cells were fixed with paraformaldehyde, followed by staining with crystal violet for 30 min. The inserts were then rinsed with PBS, air-dried, photographed, and the number of cells was counted.

Apoptosis assay

Cells were grouped and treated as described above. For each group, 3.0×10^5 cells were harvested, resuspended thoroughly in 500 μL of binding buffer to form single-cell suspensions and then stained with 5 μL Annexin V-FITC and 5 μL propidium iodide (PI) following gentle mixing. After 15 min of incubation, the cells were analyzed by flow cytometry.

Determination of glucose consumption

The cells were grouped and treated as described above. They were seeded in 96-well culture plates, and 24 h later, the culture supernatants of each group were collected. The glucose content in the culture medium was measured using a glucose assay kit, with the absorbance (OD) values read at a wavelength of 505 nm (Bai *et al*., 2024). The glucose consumption of each group of cells was then calculated.

Real-time PCR assay

Cells were grouped and treated as described above. Total RNA was extracted, cDNA was synthesized, and PCR amplification was performed according to the manufacturer's instructions. The experimental results were calculated using the $2^{-\Delta\Delta Ct}$method. The primer sequences of genes associated with iodine metabolism are presented in Table 1.

Western blot

The cells were grouped and treated as described above. Electrophoresis, electrotransfer, blocking with skim milk powder, washing with Tris-buffered saline with Tween 20 (TBST) buffer, incubation with primary antibodies [Thyroid peroxidase (TPO) (SANTA, sc-376876, 1:500), Thyroid-stimulating hormone receptor (TSHR) (SANTA, sc-53542, 1:500), Thyroglobulin (TG) (Abcam, ab156008, 1:10000), NIS (Bioss, bs-0448R, 1:500), GLUT1 (Bioss, bs-0472R, 1:1000), Acetylated Histone (AC-Histone) (CST, 13944, 1:1000), Histone (Bioss, bs-3776R, 1:1000), phosphorylated extracellular regulated protein kinase (p-ERK) (Bioss, bs-3016R, 1:1000), total extracellular

regulated protein kinase (t-ERK) (CST, 4695, 1:1000), BCL-2-associated X protein (BAX) (Proteintech, 50599-2-lg, 1:1000), B-cell lymphoma-2 (BCL-2) (Proteintech, 26593-1-AP, 1:1000), Matrix metallopeptidase 9 (MMP9) (Proteintech, 10375-2-AP, 1:500)], rinsing with TBST buffer, incubation with secondary antibody (1:2000), and ECL visualization were performed. Grayscale values were analyzed using Image Lab 5.2 software.

Immunofluorescence assay to localize NIS protein

Cells were grouped and treated as described above. Fixative was added and incubated for 10 min, followed by three washes. After blocking for 1 h, the cells were incubated with a primary antibody against NIS (1:200) and then with a fluorescent secondary antibody (1:1000). After five washes, the cells were stained with 4',6-diamidino-2-phenylindole (DAPI) for 15 min and subsequently observed under a laser confocal microscope.

Statistical analysis

Experimental data were collected and analyzed using SPSS 24.0. Intergroup comparisons were performed using one-way ANOVA. Results are expressed as mean ± SD, and $P < 0.05$ was considered statistically significant. Statistical graphs were generated using GraphPad Prism (Version 8).

RESULTS

Effects of Ve and Pa on the proliferation of FRO and ARO cells

FRO and ARO cells were treated with varying concentrations of Ve or Pa for 24 h and showed enhanced cell inhibition with increasing concentration in all groups (Fig. 1). Specifically, the inhibition rate of FRO cells reached (21.4±3.0)% at a Ve concentration of 12.5 μM, while that of ARO cells was (21.2±1.3)% at 4 μM Ve. For Pa, the inhibition rate of FRO cells was (25.0±3.0)% at 4 μM and ARO cells showed an inhibition rate of (21.8±1.2)% at 1 μM Pa.

Drug combination analysis

The combination effects of Ve and Pa were evaluated using CompuSyn software. For FRO and ARO cells, fixed concentration ratios of (12.5/4=3.125:1) and (4/1=4:1) were adopted, respectively, to determine the combined treatment doses: (6.25+2, 12.5+4, 25+8, 50+16, 100+32) μM for FRO cells and (4+1, 8+2, 16+4, 32+8, 64+16) μM for ARO cells. When Ve and Pa were combined to treat FRO and ARO cells, CI < 1, DRI > 1 and the Fa value in isobologram indicated a synergistic inhibition of proliferation (Fig. 2). Consequently, for subsequent experiments, FRO cells were treated with Ve (12.5μM) and Pa (4μM) either alone or in combination (CI = 0.26, Fa = 0.55), while ARO cells were treated with Ve (4μM) and Pa (1μM) either alone or in combination (CI = 0.12, Fa = 0.44).

Effects of Ve and Pa on clone formation and wound healing of FRO and ARO cells

Compared with the control group, the other three drug-treated groups showed significant reductions in both clone formation rate and wound healing rate (all $P<0.001$). Furthermore, the Ve+Pa combination group exhibited lower cell clone formation rate and wound healing rate than either the Ve alone group or the Pa alone group (For FRO cells, in terms of cloning results, $P = 0.049$ when compared with the Pa group. For ARO cells, in terms of cloning results, $P = 0.034$ when compared with the Pa group; for all other results, $P <0.001$) (Fig. 3).

Effects of Ve and Pa on the invasion and migration of FRO and ARO cells

Compared with the control group, the other three drug-treated groups showed significant reductions in cell migration and invasion abilities ($P<0.001$). Moreover, the Ve+Pa combination group exhibited lower cell migration and invasion abilities than either the Ve alone group or the Pa alone group (in FRO cells, for the number of migrating cells, $P = 0.02$ when compared with the Ve group and $P = 0.021$ when compared with the Pa group. For all other comparison results, $P<0.001$.) (Fig. 4).

Effects of Ve and Pa on FRO and ARO cell apoptosis

Flow cytometry analysis revealed that the Ve, Pa and Ve+Pa groups all induced apoptosis in FRO and ARO cells within 24 h. Notably, the Ve+Pa combination group significantly increased the rates of both early and late apoptosis in FRO and ARO cells (all $P<0.001$) (Fig. 5).

Effects of Ve and Pa on glucose consumption in FRO and ARO cells

Compared with the control group, the glucose consumption of both FRO and ARO cells decreased after 24 h treatment in the three other groups ($P=0.026$, $P=0.022$, $P<0.001$ for FRO cells; $P=0.028$, $P=0.012$, $P<0.001$ for ARO cells). Furthermore, the reduction in glucose consumption was more significant in the Ve+Pa combination group compared with the single-agent groups (Ve or Pa). Specifically, in FRO cells, significant differences were observed when compared with the Ve group ($P=0.018$) and the Pa group ($P=0.020$); in ARO cells, significant differences were noted when compared with the Ve group ($P=0.006$) and the Pa group ($P = 0.013$). (Fig. 6)

The expressions of FRO and ARO cell-related genes and proteins

Compared with the control group, as well as the Ve and Pa monotherapy groups, the Ve+Pa combination therapy group showed significantly increased expression levels of iodine metabolism-related genes (TSHR, TPO, TG, and NIS) (all $P<0.001$) and significantly decreased GLUT1 gene and protein expression ($P<0.001$). Compared with the control group and the Ve and Pa monotherapy groups, the Ve+Pa combination therapy group exhibited significantly increased expression levels of iodine metabolism-related proteins (TSHR, TPO, TG and NIS). Specifically, in FRO cells, the comparison results for NIS protein versus the Pa group were $P = 0.049$; the comparison of TG protein yielded $P = 0.002$; all other comparison yielded $P<0.001$. (Fig. 7).

Table 1: Primer sequence

Name	Sequence	Length (bp)	Tm (℃)
GAPDH	Forward：5’- GGAGCGAGATCCCTCCAAAAT-3’	21	59.86
	Reverse：3’- GGCTGTTGTCATACTTCTCATGG-5’	23	59.38
NIS	Forward：5’- GCAGTACATTGTAGCCACGAT-3’	21	58.45
	Reverse：3’- TGCAGATAATTCCGGTGGACA-5’	21	59.44
TG	Forward：5’-AGGGAGAGTTTATGCCTGTCC-3’	21	59.16
	Reverse：3’-CAATACCCAGATACCTCAGGGAA-5’	23	59.03
TPO	Forward：5’- GCCAACAAGCGGAGTGATTG-3’	20	60.11
	Reverse：3’- GGGCAGCATGTAAGGGAGAC-5’	20	60.46
TSHR	Forward：5’-GGAATGGGGTGTTCGTCTCC-3’	20	60.11
	Reverse：3’- GCGTTGAATATCCTTGCAGGT-5’	21	58.98
GLUT1	Forward：5’-ATTGGCTCCGGTATCGTCAAC-3’	21	60.46
	Reverse：3’-GCTCAGATAGGACATCCAGGGTA-5’	23	60.76

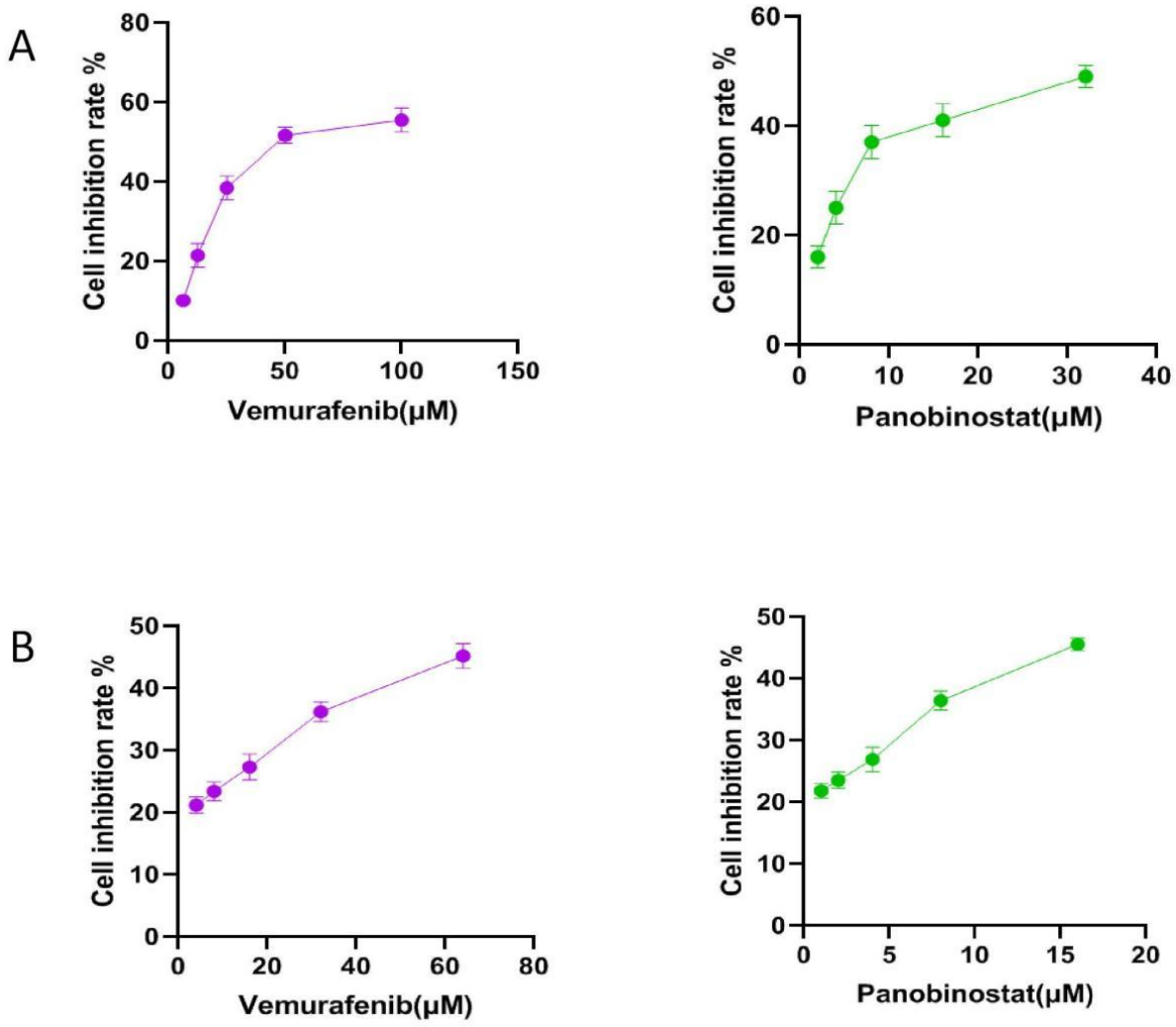

Fig. 1: Effects of different drug concentrations on FRO and ARO cell proliferation.
(A) CCK-8 assay-detected cell inhibition rates of Vemurafenib (Ve) and Panobinostat (Pa) single agents on FRO cells after 24 h treatment. (B) CCK-8 assay-detected cell inhibition rates of Ve and Pa single agents on ARO cells after 24 h treatment. Data are shown as mean ± SD, n=3.

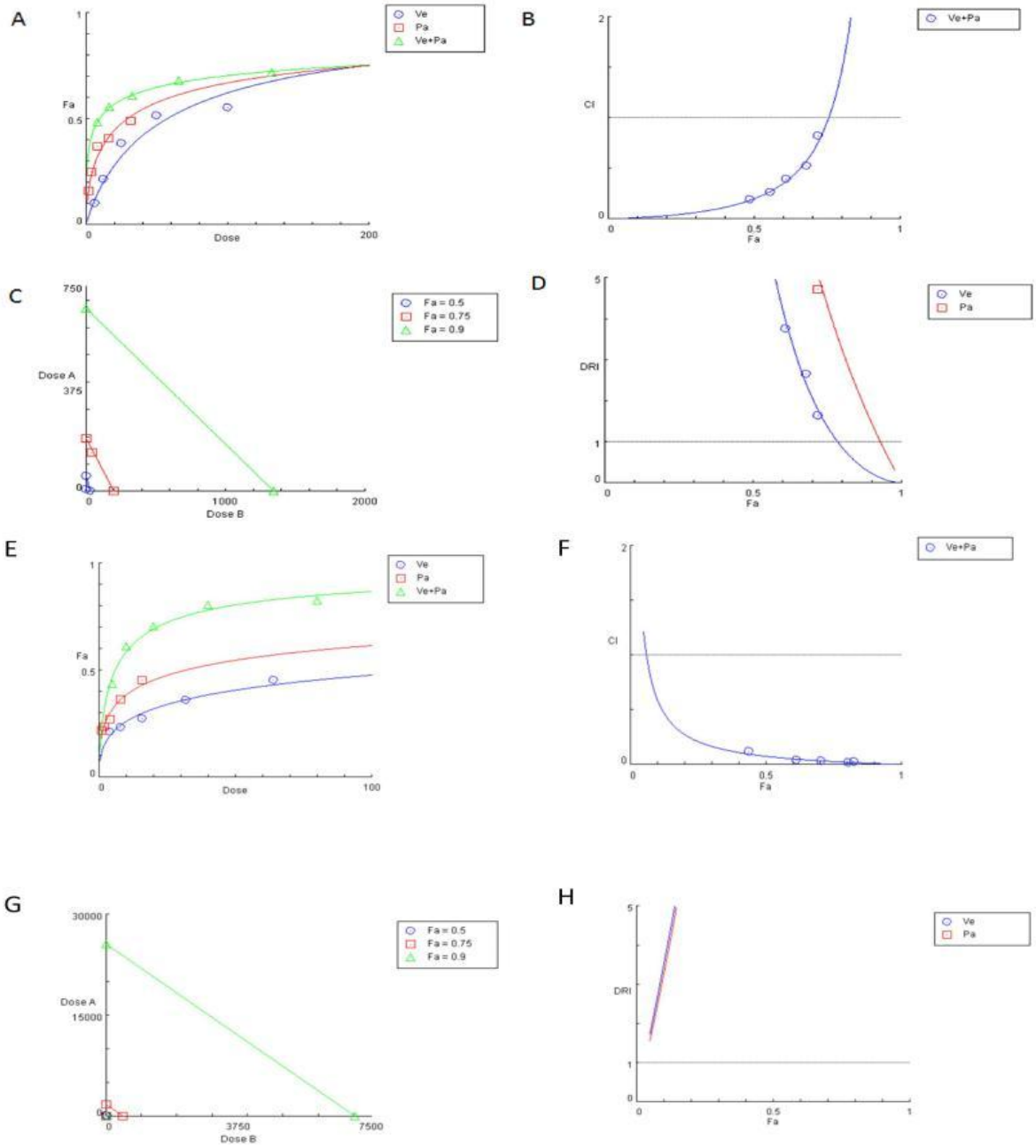

Fig. 2: CompuSyn analysis of the synergistic effect of Ve and Pa in FRO and ARO cells.
(A) Dose-effect curves of Ve, Pa, and Ve+Pa in FRO cells. (B) CI plot for Ve, Pa, and Ve+Pa in FRO cells, with a CI value < 1 indicating a synergistic interaction between Ve and Pa. (C) Isobologram analysis of Ve, Pa, and Ve+Pa in FRO cells at Fa levels of 50% (Fa 0.5), 75% (Fa 0.75), and 90% (Fa 0.9). (D) DRI of the Ve/Pa combination in FRO cells, wherein a DRI value > 1 denotes a superior therapeutic effect of the combined treatment. (E) Dose-effect curves of Ve, Pa, and Ve+Pa in ARO cells. (F) CI plot for Ve, Pa, and Ve+Pa in ARO cells, with a CI value < 1 indicating a synergistic interaction between Ve and Pa. (G) Isobologram analysis of Ve, Pa, and Ve+Pa in ARO cells at Fa levels of 50% (Fa 0.5), 75% (Fa 0.75), and 90% (Fa 0.9). (H) DRI of the Ve/Pa combination in ARO cells, wherein a DRI value > 1 denotes a superior therapeutic effect of the combined treatment.

Additionally, the expression of GLUT1 protein was significantly decreased ($P < 0.001$). Furthermore, both the Pa monotherapy group and the Ve+Pa combination therapy group showed a significant increase in AC-Histone H3 (all $P < 0.001$). Although the Ve and Pa monotherapy groups had reduced p-ERK levels, the decrease was more significant in the Ve+Pa combination therapy group (all $P < 0.001$). Moreover, compared with the control group, Ve group and Pa group, the Ve+Pa combination therapy group had elevated BAX expression and reduced BCL-2 and MMP9 expression (all $P < 0.001$) (Fig. 7).

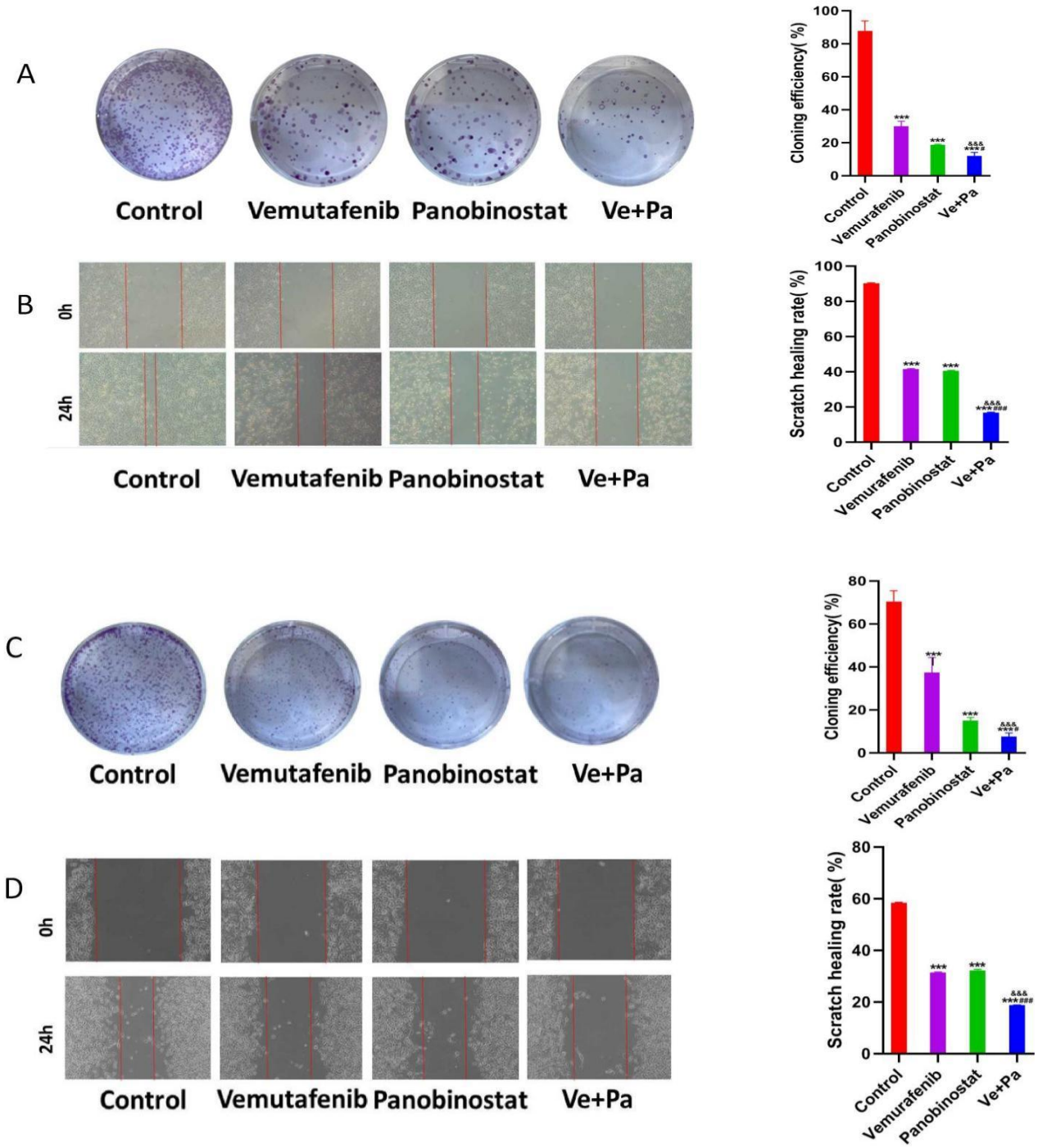

Fig. 3: Effects of Ve, Pa and Ve+Pa on colony formation and wound healing of FRO and ARO cells.
(A, C) Colony formation of FRO (A) and ARO (C) cells in the control, Ve, Pa and Ve+Pa groups at day 10. (B, D) Wound healing of FRO (B) and ARO (D) cells in the four groups. Data are presented as mean ± SD, n=3. Compared with control group, ***P<0.001, compared with Ve, $^{\&}P$<0.05, $^{\&\&\&}P$<0.001 and compared with Pa groups, $^{\#}P$<0.05, $^{\#\#\#}P$<0.001.

Immunofluorescence assay for NIS protein expression in FRO and ARO cells

In the Ve, Pa and Ve+Pa groups, both cell types exhibited increased NIS expression levels, with the Ve+Pa combination group showing a more significant elevation (all P < 0.001) (Fig. 8).

DISCUSSION

ATC is highly aggressive, currently incurable and closely associated with patient mortality (Wu *et al*., 2023). For ATC with BRAF mutations, combination drug therapy may represent a new therapeutic approach.

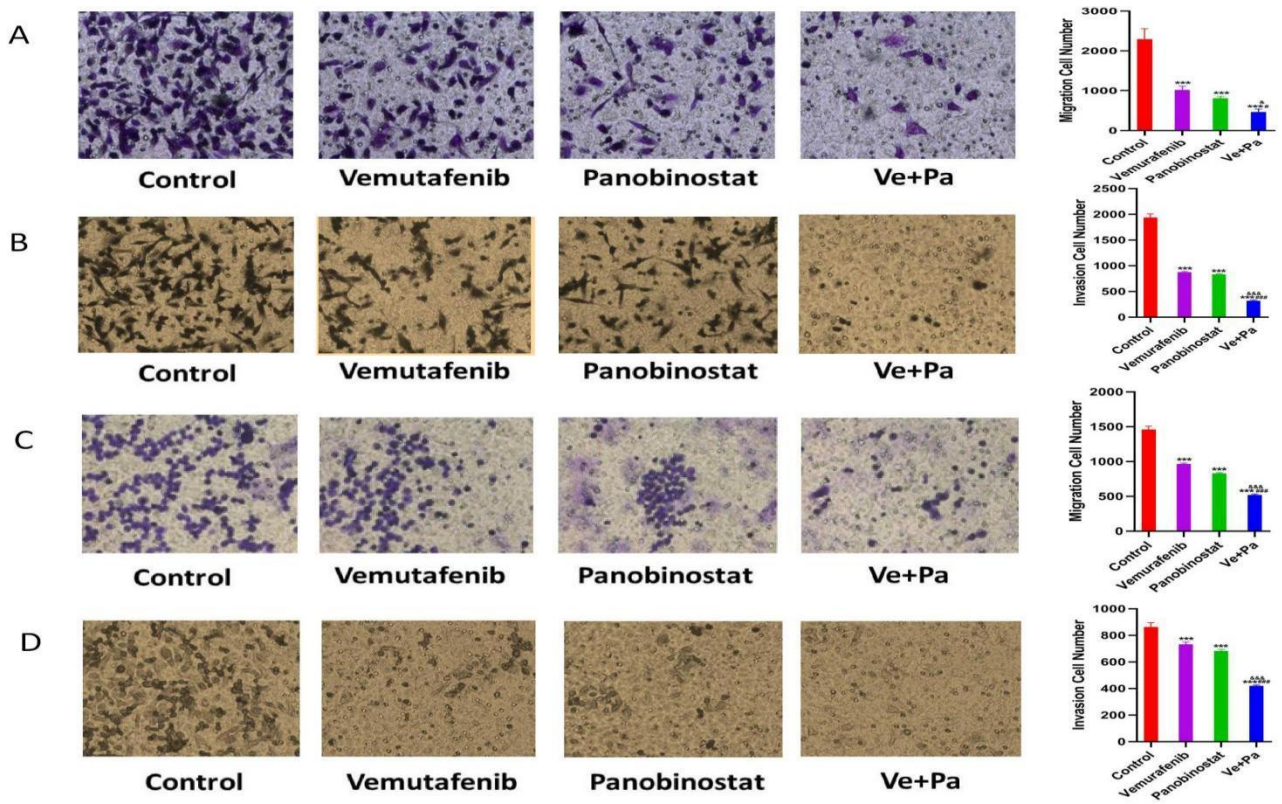

Fig. 4: Effects of Ve, Pa and Ve+Pa on the migration and invasion abilities of FRO and ARO cells (24 h treatment). (A) Migration ability of FRO cells in the control, Ve, Pa and Ve+Pa groups. (B) Invasion ability of FRO cells in the four groups. (C) Migration ability of ARO cells in the control, Ve, Pa and Ve+Pa groups. (D) Invasion ability of ARO cells in the four groups. Data are presented as mean ± SD, n=3. Compared with control group, ***$P < 0.001$, compared with Ve, $^{\&}P < 0.05$, $^{\&\&\&}P < 0.001$ and compared with Pa groups, $^{\#}P < 0.05$, $^{\#\#\#}P < 0.001$.

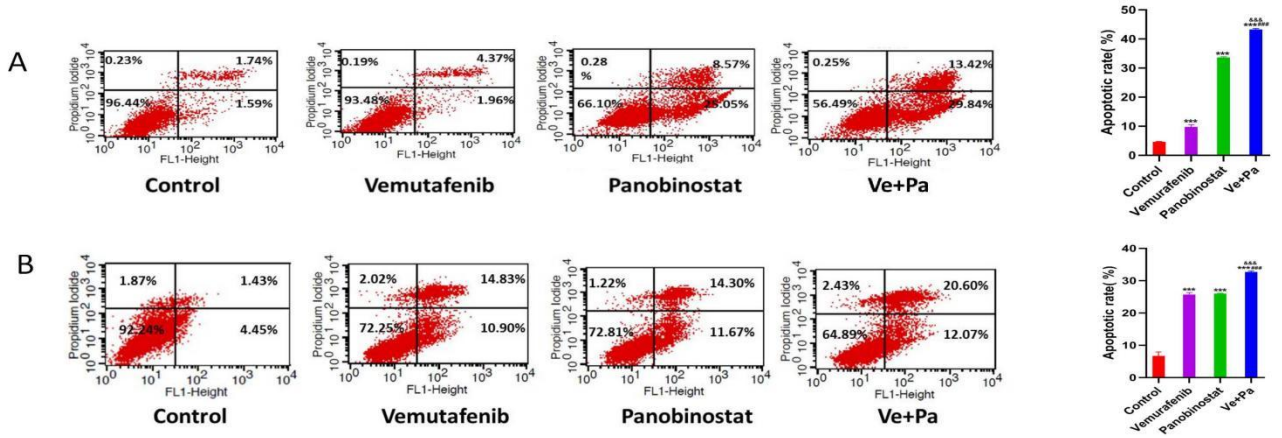

Fig. 5: Effects of Ve, Pa, and Ve+Pa on apoptosis in FRO and ARO cells after a 24-h treatment. (A, B) Representative flow cytometry plots showing early and late apoptotic cells in (A) FRO and (B) ARO cells treated with Control, Ve, Pa, or Ve+Pa. Data are presented as mean ± SD, n=3. Compared with the control group, ***P<0.001; compared with Ve, $^{\&\&\&}P < 0.001$ and compared with Pa groups, $^{\#\#\#}P < 0.001$.

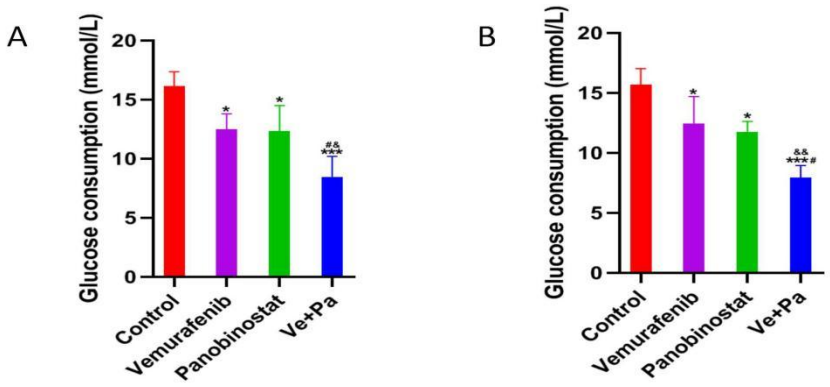

Fig. 6: Effects of Ve, Pa, and Ve+Pa on glucose consumption in FRO and ARO cells after a 24-h treatment. (A) Glucose consumption in FRO cells. (B) Glucose consumption in ARO cells. Data are presented as mean ± SD, n=3. Compared with control group, $^{*}P < 0.05$, $^{***}P < 0.001$, compared with Ve, $^{\&}P < 0.05$, $^{\&\&\&}P < 0.01$ and compared with Pa groups, $^{\#}P < 0.05$.

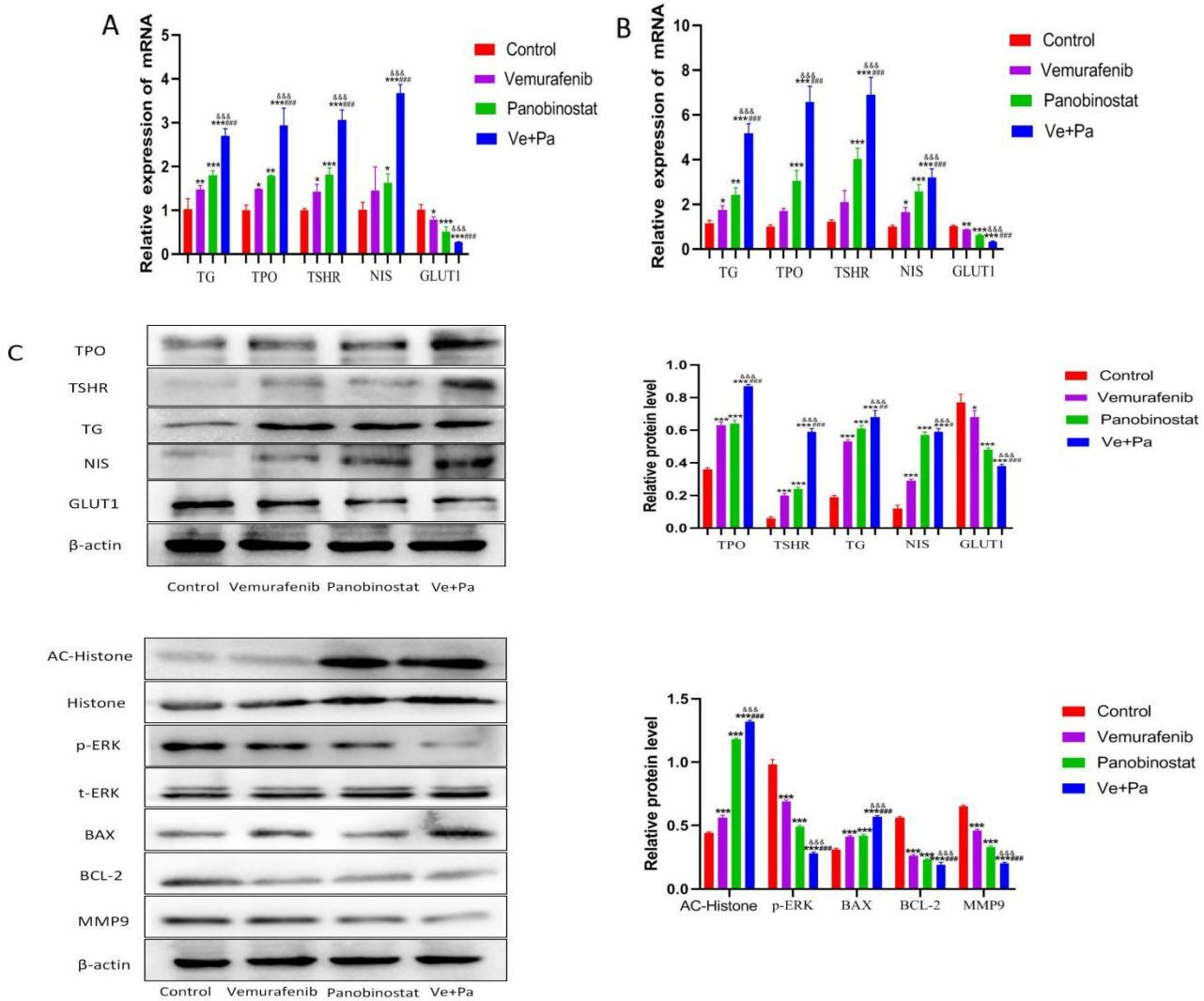

Fig. 7 is continue…

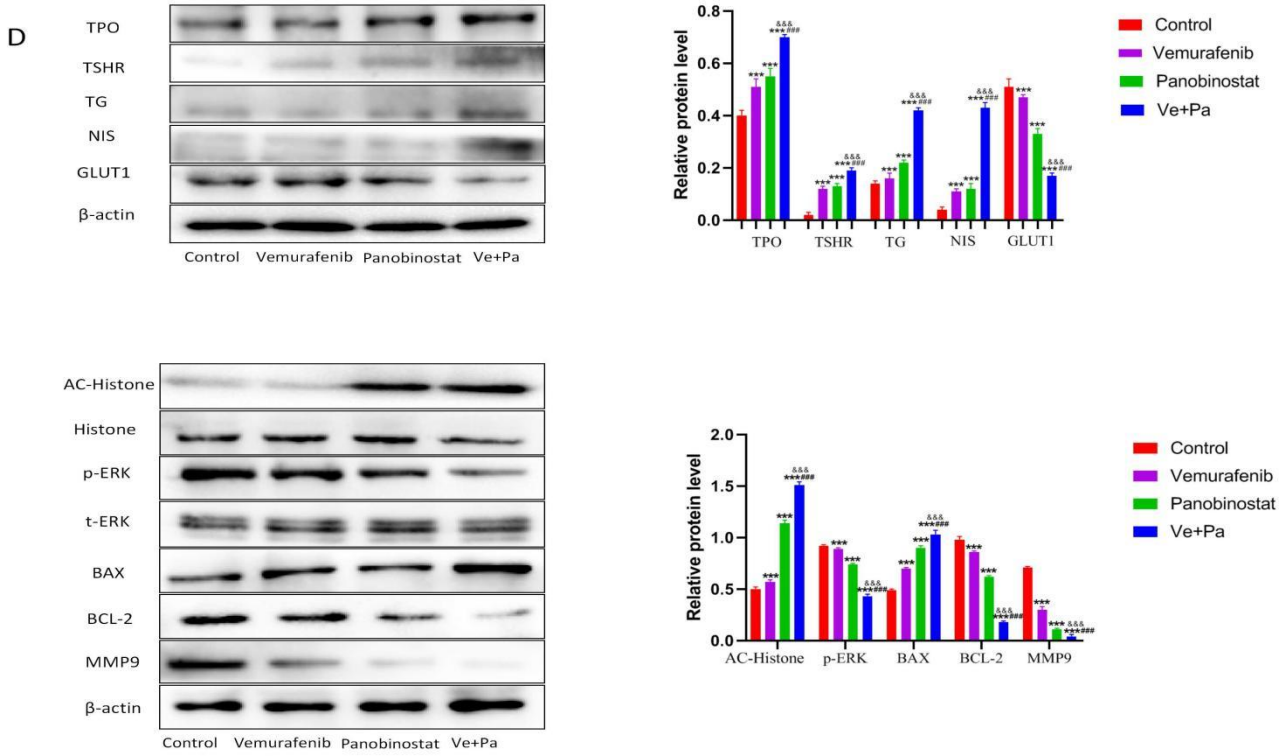

Fig. 7: Effects of Ve, Pa, and Ve+Pa on gene and protein expression in FRO and ARO cells after a 24-h treatment. (A, B) qRT-PCR analysis of thyroid hormone synthesis-related gene expression (THSR, TPO, TG, NIS, GLUT1) in (A) FRO and (B) ARO cells. (C, D) Western blot analysis of proteins involved in iodine metabolism, glucose metabolism, and apoptosis in (C) FRO and (D) ARO cells. Data are presented as mean ± SD, n=3. Compared with control group, $^{*}P < 0.05$, $^{**}P < 0.01$, $^{***}P < 0.001$, compared with Ve, $^{\&}P < 0.05$, $^{\&\&}P < 0.01$, $^{\&\&\&}P < 0.001$ and compared with Pa groups, $^{\#}P < 0.05$, $^{\#\#}P < 0.01$, $^{\#\#\#}P < 0.001$.

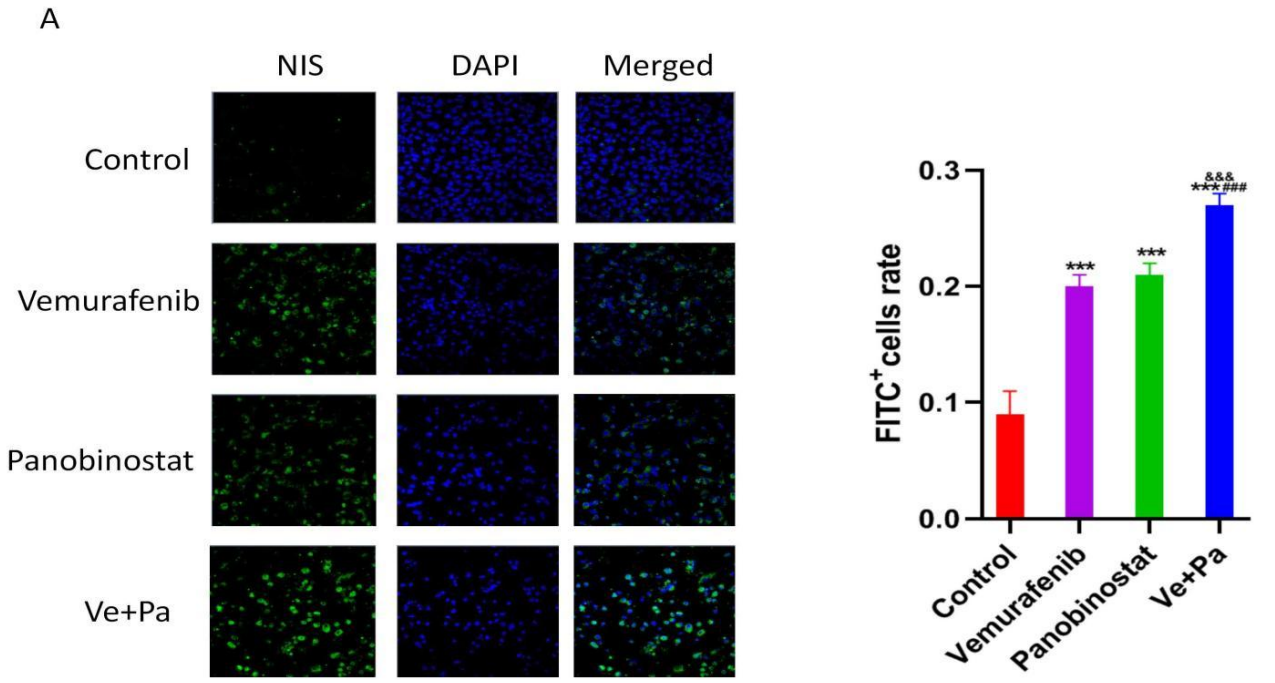

Fig. 8 is continue…

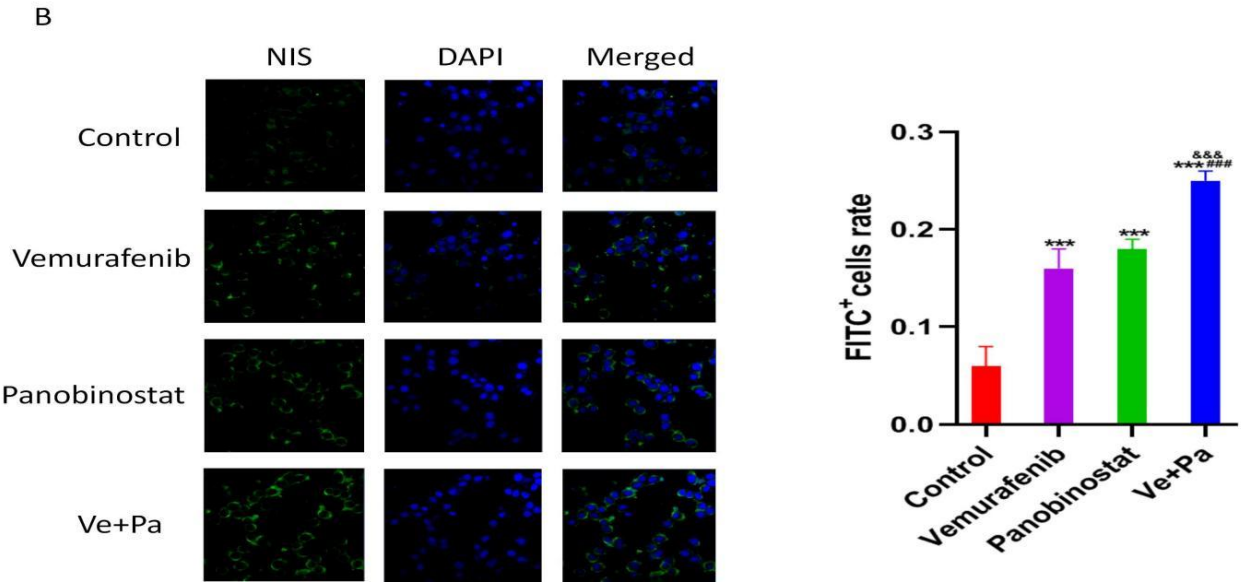

Fig. 8: Immunofluorescence analysis of NIS protein expression in FRO and ARO cells after treatment with Ve, Paand Ve+Pa.
(A) Representative immunofluorescence images of FRO cells stained with DAPI (blue, nuclear marker) and NIS-specific antibody (green) in the control, Ve, Pa and Ve+Pa groups. (B) Representative immunofluorescence images of ARO cells stained with DAPI (blue, nuclear marker) and NIS-specific antibody (green) in the four groups. Data are presented as mean ± SD, n=3. Compared with control group, $^{***}P < 0.001$, compared with Ve, $^{\&\&\&}P < 0.001$ and compared with Pa groups, $^{\#\#\#}P < 0.001$.

Researchers have found that the synergistic effect of trametinib and alpelisib can inhibit the MAPK and PI3K/AKT/mTOR pathways, thereby targeting tumor cells harboring BRAF mutations (Chen *et al*., 2024). Ve, a BRAF V600E inhibitor, can disrupt this signaling pathway and reduce tumor volume in several malignancies. Studies have confirmed its antitumor effect in TC (Lang *et al*., 2023). However, Ve can upregulate VCAM-1 in thyroid cancer cells, leading to resistance in BRAF-mutated TC (Chen *et al*., 2020). Studies have revealed that Ve in combination with metformin can target and regulate signaling pathways, including BRAF/ERK, in ATC cells, while significantly inducing apoptosis (Durai *et al*., 2021). Treatment of BALB/c mice with chloroquine (CQ) in combination with HDAC inhibitors resulted in increased levels of NIS mRNA in thyroid tissues (Read *et al*., 2024).

Pa is a novel HDAC inhibitor; the combination of PD-L1 inhibitors with Pa and sorafenib exerts a synergistic effect, significantly reducing the survival rate of ATC cells (Wächter *et al*., 2023). The present study shows that the combination of Ve and Pa effectively inhibits the proliferation of FRO and ARO cells, promotes apoptosis, upregulates BAX expression, downregulates BCL-2 expression, and reduces MMP9 levels, thereby decreasing the invasive and metastatic capabilities of the cells. NIS is localized on the basolateral membrane, mediating the active transport of iodine from the bloodstream into thyroid follicular cells. Meanwhile, the reduction in iodine uptake is closely associated with the presence of NIS in the cytoplasm and post-translational regulation (Oh *et al*., 2021). In the present study, treatment of $BRAF^{V600E}$ mutated FRO and ARO cells (Chen *et al*., 2020; Du *et al*., 2022) with the HDAC inhibitor Pa combined with the BRAF inhibitor Ve resulted in increased histone acetylation, significantly elevated NIS expression and decreased p-ERK expression. Compared with single-drug treatments, the combination also significantly upregulated the expression of iodine metabolism-related genes (TG, TPO and TSHR), thereby inducing cell differentiation. These findings indicate that in $BRAF^{V600E}$ mutated thyroid cancer, the combination of Pa and Ve enhances histone acetylation and inhibits the MAPK signaling pathway, which collectively promotes the expression of iodine metabolism-related genes and increases the potential for cell redifferentiation. Studies have demonstrated that overexpression of GLUT1/3 is associated with the aggressiveness of oral tumors, including their invasiveness and drug resistance. Notably, blocking the GLUT1 receptor can sensitize CisR-OSCC cells (Kumari *et al*., 2023). In this study, either BRAF inhibitors or HDAC inhibitors alone could reduce GLUT1 expression, but the combined treatment exerted a more pronounced effect. The findings demonstrated that for FRO and ARO cells harboring the $BRAF^{V600E}$ mutation, the combination of Ve and Pa produced a significant synergistic effect: it markedly inhibited cell proliferation, increased apoptosis rates and

thereby reduced cell migration and invasion capabilities. Meanwhile, this combination regimen effectively upregulated the expression of iodine metabolism-related genes, downregulates the expression of glucose transporters, reduces glucose consumption and induces cell differentiation. This study provides a theoretical basis for the application of targeted drug combination therapy in TC patients with the $BRAF^{V600E}$ mutation.

To date, this study has only verified the synergistic effect of the combination of Ve and Pa through *in vitro* cell experiments. Such experiments merely reflect the direct effects of the drugs on specific cancer cells, whereas the in vivo environment may significantly impact drug efficacy. In summary, the research team will establish relevant animal models in subsequent studies to validate the in vivo tumor-suppressive effect, safety and dosage optimization scheme of this combination therapy. This will provide a basis for the translation of basic research into clinical treatment.

CONCLUSION

In this study, we demonstrated that Ve and Pa exert a synergistic effect in inhibiting the growth and metastasis of FRO and ARO cells, while concurrently promoting their apoptosis and differentiation. These findings provide a theoretical foundation for the application of targeted combination drug therapy in patients with TC.

Acknowledgments
None.

Authors' contribution
Yang Li: Writing – review and editing, writing – original draft, resources, methodology, investigation, formal analysis, data curation and conceptualization. Han Gao: Writing – review and editing, writing – original draft and Resources. Peng Zhang: Methodology, investigation, formal analysis, data curation and conceptualization. Wenjun Wang: Methodology. Jianwen Zhou: Investigation, formal analysis, data curation and conceptualization. Jing Cui: Investigation, resources and methodology. Di Xue: Data curation. Baofeng Zhang: Formal analysis, data curation and conceptualization. Peihong Li: Writing – original draft, resources, methodology and investigation. Li Fan: Writing – review and editing, writing – original draft, visualization, supervision and resources. Jingwei Xu: Project administration, methodology, investigation, funding acquisition and data curation.

Funding
This study was supported by: Scientific Research Project of Heilongjiang Provincial Health Commission (20240202040289); The Natural Science Foundation of Heilongjiang Province (PL2024H258); Qiqihar Science and Technology Plan Joint Guidance Project (LSFGG-2024107), (LSFGG-2022057) and (LSFGG-2025093) ; Research project of basic research business expenses of provincial colleges and universities in Heilongjiang Province (2021-KYYWF-0362) and (2023-KYYWF-0856); Traditional Chinese Medicine Research Project of Heilongjiang Province (NO.ZHY2024-279); Graduate Innovation Fund Project of Qiqihar Medical University (QYYCX2023-51), (QYYCX2024-54) and (QYYCX2024-56).

Data availability statement
The datasets generated during and/or analysed during the current study are available from the corresponding author on reasonable request.

Ethical approval
The present study was limited to *in-vitro* cell experiments and did not involve any animal or human experimental procedures; therefore, ethical approval was deemed unnecessary.

Conflict of interest
The authors have no conflicts of interest to declare.

REFERENCES

Boucai L, Zafereo M and Cabanillas ME (2024). Thyroid Cancer: A Review. *JAMA*., **331**(5): 425-435.

Bhutkar S, Yadav A, Patel H, Barot S, Patel K and Dukhande VV (2024). Synergistic efficacy of CDK4/6 inhibitor abemaciclib and HDAC inhibitor panobinostat in pancreatic cancer cells. *Cancers (Basel)*., **16**(15): 2713.

Bai J, Wang Z, Yang M, Xiang J and Liu Z (2024). Disrupting CENP-N mediated SEPT9 methylation as a strategy to inhibit aerobic glycolysis and liver metastasis in colorectal cancer. *Clin Exp Metastasis.,* **41**(6):971-988.

Chang S, Xiao W, Xie Y, Xu Z, Li B, Wang G, Hu K, Zhang Y, Zhou J, Song D, Zhu H, Wu X, Lu Y, Shi J and Zhu W (2023). TI17, a novel compound, exerts anti-MM activity by impairing Trip13 function of DSBs repair and enhancing DNA damage. *Cancer Med*., **12**(23): 21321-21334.

Chen CP, Lin SF, Yeh CN, Huang WK, Pan YR, Hsiao YT, Lo CH and Wu CE (2024). Synergistic effects of the combination of trametinib and alpelisib in anaplastic thyroid cancer with BRAF and PI3KCA co-mutations. *Heliyon*., **10**(7): e29055.

Chen S, Su X, Jiang X, Zhang T, Min I, Ding Y, Wang X, Mao Z, Cao J, Teng X, Fahey TJ 3rd, Wang W and Teng L (2020). VCAM-1 Upregulation contributes to insensitivity of vemurafenib in BRAF-mutant thyroid cancer. *Transl. Oncol*., **13**(2): 441-451.

Durai L, Ravindran S, Arvind K, Karunagaran D and Vijayalakshmi R (2021). Synergistic effect of metformin and vemurufenib (PLX4032) as a molecular targeted therapy in anaplastic thyroid cancer: An *in-vitro* study. *Mol. Biol. Rep*., **48**(11): 7443-7456.

Du L, Zhao Q, Li J, Wang M and Qiao H (2022).

Expression of colorectal neoplasia differentially expressed in anaplastic thyroid carcinoma and its effect on cancer cell proliferation. *Ann. Transl. Med*., **10**(8): 473.

Faria M, Domingues R, Bugalho MJ, Matos P, Silva AL (2021). MAPK inhibition requires active rac1 signaling to effectively improve iodide uptake by thyroid follicular cells. *Cancers (Basel).*, **13**(22): 5861.

Hu Y, Wen Q, Cai Y, Liu Y, Ma W, Li Q, Song F, Guo Y, Zhu L, Ge J, Zeng Q, Wang J, Yin C, Zheng G and Ge M (2023). Alantolactone induces concurrent apoptosis and GSDME-dependent pyroptosis of anaplastic thyroid cancer through ROS mitochondria-dependent caspase pathway. *Phytomedicine*., **108**:154528.

Ismail J, Shebaby W, Azar Atallah S, Taleb RI, Kawrani S, Faour W and Mroueh M (2025). Combination of cannabidiol with cisplatin or paclitaxel analysis using the chou-talalay method and chemo-sensitization evaluation in platinum-resistant ovarian cancer cells. *Biomedicines.,* **13**(2):520.

Kopetz S, Guthrie KA, Morris VK (2021). Randomized Trial of irinotecan and cetuximab with or without vemurafenib in BRAF-mutant metastatic colorectal cancer (SWOG S1406). *J. Clin. Oncol.,* **39**(4): 285-294.

Kumari A, Jha A, Tiwari A, Nath N, Kumar A, Nagini S and Mishra R (2023). Role and regulation of GLUT1/3 during oral cancer progression and therapy resistance. *Arch. Oral Biol*., **150**: 105688.

Lawless AK, Kumar S, Bindra J, Sywak M, Chou A, Turchini J, Papachristos A, Wijewardene A, Sidhu S, Ahadi M, Tacon L, Glover A, Clark K, Tsang V, Pang L, Clifton-Bligh RJ, Robinson B, Gill AJ, Guminski A, Eade T and Gild ML (2024). Anaplastic thyroid cancer: A review of recent evidence and summary of an Australian institutional protocol. *Asia Pac. J. Clin. Oncol*., **20**(6): 681-689.

Lu MD, Li H, Nie JH, Li S, Ye HS, Li TT, Wu ML, Liu J (2022). Dual inhibition of BRAF-MAPK and STAT3 signaling pathways in resveratrol-suppressed anaplastic thyroid cancer cells with BRAF mutations. *Int. J. Mol. Sci*., **23**(22): 14385.

Lang M, Longerich T and Anamaterou C (2023). Targeted therapy with vemurafenib in BRAF (V600E)-mutated anaplastic thyroid cancer. *Thyroid Res*., **16**(1): 5.

Mihailovic J, Killeen RP, Duignan JA (2021). PET/CT variants and pitfalls in head and neck cancers including thyroid cancer. *Semin Nucl Med*., **51**(5): 419-440.

Pliszka M and Szablewski L (2021). Glucose transporters as a target for anticancer therapy. *Cancers (Basel)*., **13**(16): 4184.

Oh JM and Ahn BC (2021). Molecular mechanisms of radioactive iodine refractoriness in differentiated thyroid cancer: Impaired sodium iodide symporter (NIS) expression owing to altered signaling pathway activity and intracellular localization of NIS. *Theranostics*., **11**(13): 6251-6277

Rathod M, Kelkar M, Valvi S, Salve G and De A (2020). FOXA1 regulation turns benzamide HDACi treatment effect-specific in BC, promoting NIS gene-mediated targeted radioiodine therapy. *Mol. Ther. Oncolytics*., **19**: 93-104.

Read ML, Brookes K, Zha L, Manivannan S, Kim J, Kocbiyik M, Fletcher A, Gorvin CM, Firth G, Fruhwirth GO, Nicola JP, Jhiang S, Ringel MD, Campbell MJ, Sunassee K, Blower PJ, Boelaert K, Nieto HR, Smith VE and McCabe CJ (2024). Combined vorinostat and chloroquine inhibit sodium-iodide symporter endocytosis and enhance radionuclide uptake in-vivo. *Clin. Cancer Res*., **30**(7): 1352-1366.

Scheffel RS, Dora JM, Maia AL (2022). BRAF mutations in thyroid cancer. *Curr. Opin. Oncol*., **34**(1): 9-18.

Su X, Li P, Han B, Jia H, Liang Q, Wang H, Gu M, Cai J, Li S, Zhou Y, Yi X and Wei W (2021). Vitamin C sensitizes BRAFV600E thyroid cancer to PLX4032 via inhibiting the feedback activation of MAPK/ERK signal by PLX4032. *J. Exp. Clin. Cancer Res*., **40**(1): 34.

Wu SS, Lamarre ED, Yalamanchali A, Brauer PR, Hong H, Reddy CA, Yilmaz E, Woody N, Ku JA, Prendes B, Burkey B, Nasr C, Skugor M, Heiden K, Chute DJ, Knauf JA, Campbell SR, Koyfman SA, Geiger JL and Scharpf J (2023). Association of treatment strategies and tumor characteristics with overall survival among patients with anaplastic thyroid cancer: A single-institution 21-year experience. *JAMA Otolaryngol. Head Neck Surg*., **9**: e225045.

Wachter S, Knauff F, Roth S, Keber C, Holzer K, Manoharan J, Maurer E, Bartsch DK and Di Fazio P (2023). Synergic induction of autophagic cell death in anaplastic thyroid carcinoma. *Cancer Invest*., **41**(4): 405-421.